This article has been accepted for publication in Physical Review B (M. Kuzmin, J.-P. Lehtiö, Z. J. Rad, S. V. Sorokina, M. P. J. Punkkinen, P. Laukkanen, and K. Kokko Atomic and electronic structures of Si/Ge(100) interfaces studied by high-resolution photoelectron spectroscopy and scanning tunneling microscopy) Phys. Rev. B 103, 195312 – Published 21 May 2021) https://doi.org/10.1103/PhysRevB.103.195312 Copyright © 2021 by American Physical Society. All rights reserved.

Atomic and electronic structures of Si/Ge(100) interfaces studied by high-resolution photoelectron spectroscopy and scanning tunneling microscopy

M. Kuzmin,[1,2,*] J.-P. Lehtiö,[1] Z. J. Rad,[1] S. V. Sorokina,[2] M. P. J. Punkkinen,[1] P. Laukkanen,[1] and K. Kokko[1]
[1]*Department of Physics and Astronomy, University of Turku, FI-20014 Turku, Finland*
[2]*Ioffe Physical-Technical Institute, Russian Academy of Sciences, St. Petersburg 194021, Russian Federation*

(Received 10 April 2021; accepted 10 May 2021; published 21 May 2021)

The close similarity of silicon and germanium, isoelectronic group-IV elements, makes the integration of Ge layers on Si substrates suitable for technology development, but the atomic and electronic structures of $Si_{1-x}Ge_x$ surfaces are still an open issue, in particular, for the alloy systems where Si is deposited on the Ge substrate. In this study, utilizing low-energy electron diffraction, scanning tunneling microscopy, and photoelectron spectroscopy using synchrotron radiation, we demonstrate that the formation mechanisms of the Si-on-Ge structures are controlled by two interface phenomena, namely Si indiffusion and Ge segregation on top of this surface. Employing these phenomena and controlling the Si quantity, one can synthesize the well-defined crystalline Ge-(2 × 1)/$Si_{1-x}Ge_x$/Ge(100) stacks where the number of Si atoms at the host Ge lattice sites can be tuned. Using the obtained data on the atomic and electronic structures of such systems, we also propose a method for interface engineering of Ge/Si/Ge stacks with tailored properties as promising templates for growing the device junctions.

DOI: 10.1103/PhysRevB.103.195312

I. INTRODUCTION

Germanium and silicon are closely related isoelectronic group-IV materials that are completely miscible over the full range of $Si_{1-x}Ge_x$ compositions (i.e., for x from 0 to 1). However, the bulk lattice constants are clearly different: 5.66 Å for Ge and 5.43 Å for Si. It can be expected that the aforementioned difference (4.2%) is a key factor behind the formation mechanisms and physical properties of SiGe materials for the Ge epitaxial growth on Si [1]. The lattice mismatch at the interface between the $Si_{1-x}Ge_x$ layer and Si can be accommodated either by compression of $Si_{1-x}Ge_x$ or by the introduction of misfit dislocations at the interface.

Likewise, one could tentatively expect that when Si is deposited on a Ge substrate, the most remarkable difference is that the compressive strain in the deposited layer is replaced by tensile strain, while the physical processes at the interface have still remained qualitatively unchanged. However, contrary to this expectation, the Si-on-Ge interface represents a significantly more complicated system. Lin *et al.* [2] have found that the top layer of Ge(100) after the deposition of several atomic layers of Si at 450 °C is still terminated by Ge atoms, whereas the Si atoms move below the surface, and that this tendency persists for growth at about room temperature (RT). The surface segregation of Ge can be tentatively understood on the basis of *ab initio* total-energy calculations indicating that the Ge(100) surface has a lower surface free energy than the Si(100) surface [3]. Moreover, *ab initio* calculations in Ref. [4] have shown that the Ge dimers on top of the Si/Ge(100) interface are energetically favorable (by 0.38 eV per dimer) over the Si dimers on the nonsegregated Si-capped surface. In contrast, using atomic force microscopy, cross-sectional transmission electron microscopy, and x-ray diffraction, Tu *et al.* [5] have reported three-dimensional Si quantum dots on the Ge(100) at the initial stage of growth, i.e., for 4–20 monolayers (MLs). Furthermore, the complexity of Si/Ge(100) can be evidenced by the results of Leys *et al.* [6]. Using low-energy secondary ion mass spectrometry, they have shown that for thin Si films on Ge(100), the Ge segregation is controlled by the sample temperature and deposition method; in particular, such a process occurs efficiently for the Si growth from SiH_4 at 500 °C, whereas the amount of segregated Ge significantly decreases for the Si growth using Si_3H_8 at 350 °C. All in all, even though the tendency of Ge segregation in such systems has been reliably established in earlier studies, several issues have not yet been solved. For example, the structure of the subsurface region resulting from the Si indiffusion is unknown yet. Also, it is still unclear how thick the mixed Si-Ge interfaces are (we denote such an interface as the whole part of Si-adsorbed Ge substrate which is different from the bulk). Moreover, the electronic structure of Si/Ge interfaces is unclear; for instance, it is unknown whether or not very strong Fermi level pinning on the clean n-type Ge(100) [7] is alleviated by the Si deposition. These issues are important not only from the fundamental point of view but also for the SiGe-based technology.

One application example is the insulator-Ge junctions. It is well known that Ge has a weakness as a channel material in metal-oxide-semiconductor field-effect transistors, and the most essential reason is a lack of high-quality passivation of Ge surfaces [8]. Because of their poor electrical properties and solubility, Ge oxides should be removed from Ge substrates prior to metal-oxide high-k film deposition. In practice,

*m.kuzmin@mail.ioffe.ru

 ©2021 American Physical Society

however, reoxidation of Ge during the fabrication of high-*k*/Ge gate stacks is difficult to avoid. This problem can be solved by interposing a passivating layer between the high-*k* film and the Ge surface, which can lead to an improvement in the electrical properties of the stack [9]. One of the most promising materials for the interface passivation layer is silicon. Therefore, the atomic-level understanding of basic properties of Si/Ge interfaces at initial stages of its synthesis is very relevant to the technology as well. Moreover, the other intriguing example is a very recent application of Ge/SiGe heterostructure in a four-qubit germanium quantum processor using a Ge quantum well in between two $Si_{0.2}Ge_{0.8}$ layers at a depth of 55 nm from the dielectric/semiconductor interface [10]. Obviously, the physical realization of such complex systems requires detailed knowledge of Si-Ge interaction not only at surfaces but also in buried layers of various heterojunctions.

In this work, we combine low-energy electron diffraction (LEED), scanning tunneling microscopy (STM), x-ray photoelectron spectroscopy (XPS), and angle-resolved core-level (CL) and valence-band (VB) photoemission using the synchrotron radiation to investigate the atomic structure and electronic properties of Si/Ge(100) interfaces as function of growth temperature and quantity of deposited Si atoms. We demonstrate differences in structural arrangement and bonding environment for interfaces involving 1 and 4 MLs of Si atoms. In contrast, the valence-edge electronic properties of these interfaces are to a large extent controlled by the Ge bulk properties and only weakly affected by the deposited Si atoms. Finally, on the basis of obtained fundamental knowledge, we propose a different approach for interface engineering of advanced crystalline Si/Ge(100) structures that can be considered a promising candidate for a template for growing improved high-*k*/Ge junctions.

II. EXPERIMENT

The experiments were performed *in situ* in two separate ultrahigh vacuum (UHV) systems. The STM measurements were performed in the UHV system with the base pressure below 1×10^{-10} mbar, which was equipped with the Omicron STM operating at RT, LEED, XPS, and Ar^+ ion bombardment facilities. The STM images were taken with W tips in the constant-current mode at RT. The WSXM package [11] was partly utilized for processing the STM data.

The photoemission measurements were carried out at MAX-lab (beamline I4) in Lund, Sweden. The CL and VB spectra were acquired at RT by the SPECS Phoibos 100 analyzer with acceptance angles of $\pm 1^\circ$ and $\pm 9^\circ$, respectively. The energy step used for the acquisition of these spectra was 10 meV, and the instrumental resolution was better than 100 meV. The photon energy ($h\nu$) and emission angle (θ_e) were variable for optimizing the probing depth. The binding energy was determined by using a reference Ta sample in a good contact with the Ge samples. The CL spectra were quantitatively analyzed by a standard fitting procedure described elsewhere (e.g., Ref. [12]). The top of the VB in the valence spectra was determined by extrapolating linear segments of curves to the zero emission level as an offset on the energy axis.

The clean Ge(100) surfaces (*n*-type, Sb doped, $\sim 1 \times 10^{18}$–1×10^{19} cm^{-3}) were prepared by several cycles of Ar^+ ion bombardment at 400 °C and subsequent annealing at 630 °C until sharp (2×1) patterns were observed by LEED. In addition, the cleanness of pristine surfaces was verified by STM and Ge 3*d* CL spectroscopy. The Si deposition was performed from a tungsten-filament evaporator heated by direct current. The evaporator was carefully outgassed prior to the Si deposition. Its rate was calibrated by observing the attenuation of Ge 3*d* photoemission signal from the test Ge samples covered progressively by Si layers at RT as well as by estimating the ratio of covered and bare surface areas in STM images of Si(111)(7×7) with submonolayer quantities of Si atoms adsorbed at RT. One monolayer of Si atoms on Ge(100) was referred to as the atomic density on the clean substrate surface (i.e., 6.24×10^{14} cm^{-2}). During the Si deposition the sample was kept at RT. The annealing time after the deposition was 30 min. The sample temperature was measured by infrared pyrometers.

III. RESULTS AND DISCUSSION

A. Structural properties

As the structural properties of Si/Ge(100) systems are significantly affected by the amount of deposited atoms, we will denote the systems with the nominal Si coverages of 1 and 4 ML the Si_{1ML}/Ge and Si_{4ML}/Ge, respectively.

1. Si_{1ML}/Ge

At RT ~1 ML of Si atoms deposited on the clean Ge(100) surface has almost completely removed the native (2×1) reconstruction, leading to the amorphization of the upper Ge-dimer layer of substrate. Figures 1(a) and 1(b) show LEED patterns from the pristine Ge(100)(2×1) and Si-covered Ge(100) (Si_{1ML}/Ge hereafter), respectively. As seen, the intensity of (2×1) LEED spots, which are the fingerprint of native dimer-row reconstruction on the clean substrate, is significantly decreased upon the Si deposition. In contrast, the (1×1) spots have still persisted, and their intensity is nearly as bright as before the deposition, indicating that the crystallinity of Ge below the topmost layer has remained intact. This means that Si indiffusion is unlikely at RT.

The above LEED observations are supported well by STM results. Figures 2(a) and 2(b) present atomic-resolution filled-state STM images for the clean substrate and Si_{1ML}/Ge, respectively. At the chosen bias voltage ($V_S = -1.3$ V), the Ge dimers on the clean substrate usually appear in the form of bean-shaped protrusions that are an average of two possible tilting-dimer configurations [i.e., $Ge_{up} - Ge_{down}$ and $Ge_{down} - Ge_{up}$, where Ge_{up} and Ge_{down} are dimer-up and dimer-down atoms, respectively], for which a rapid switchover occurs at RT (so-called flip-flop motion) [13–15]. Locally, each configuration can be frozen by defects, etc., leading to static buckled dimers appearing in room-temperature STM as single protrusions associated with the occupied dangling-bond states caused by the Ge_{up} atoms. It is seen in Fig. 2(a) that the STM protrusions originating from the static buckled dimers produce a local $c(4 \times 2)$ periodicity where the zigzag rows are arranged in an antiferromagnetic

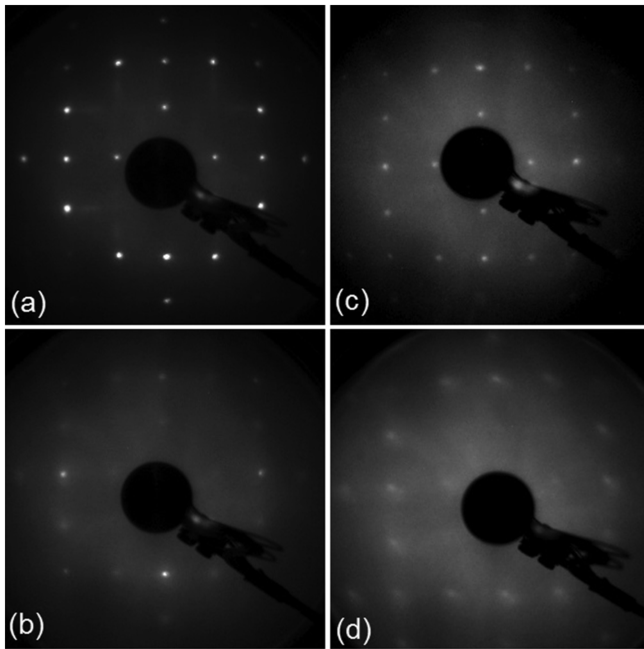

FIG. 1. LEED patterns for (a) the clean Ge(100), Si_{1ML}/Ge at (b) RT and (c) 500 °C, and (d) Si_{4ML}/Ge. The electron energy is (a) 138 eV, (b),(c) 128 eV, and (d) 108 eV.

manner [16,17]. The local character of this periodicity does not allow one to observe the respective fourfold spots in LEED at RT [Fig. 1(a)].

The STM image of Si_{1ML}/Ge in Fig. 2(b) clearly shows that the dimer row structure of Ge substrate is broken by Si deposition. There are two distinct phases on this surface; one is an amorphous structure comprised of islands appearing as brighter areas in the STM image. The top of such islands does not show any regular arrangement. The area in between such islands exhibits the other phase that appears as darker cavities and is built up of buckled dimer rows similar to those of the clean substrate. Interestingly, for most of dimers on the Si_{1ML}/Ge, the flip-flop motion is blocked in the presence of islands at RT. This blocking can be rationalized in terms of the fact that the dimer flip-flop motion is caused by a diffusing antiphase boundary, i.e., two neighboring dimers that are aligned in the same direction (the so-called phason) along the dimer rows [15]. Most likely, the presence of islands in Fig. 2(b) leads to the absence of such phasons and, therefore, the blocking of the dimer flip-flop motion on the bare Ge(100).

The origin of two phases in Fig. 2(b) can be elucidated from the roughness analysis performed on the basis of STM topography data. In height distribution shown in Fig. 2(c), the solid circles represent the number of events (points) in the STM image of Fig. 2(b), where the tip height ranges within $z \pm \Delta z$. It is seen that the distribution curve has two maxima. Such a line shape is in accordance with the presence of two phases on the Si_{1ML}/Ge surface. The curve can be reasonably fitted by two Gaussian peaks indicated by blue and green lines. The resultant fitting curve is depicted by a red line. One can assume that each Gaussian peak is ascribed to the height distribution of the corresponding surface phase found in Fig. 2(b). Namely, the blue curve is related to the upper height-level phase which is composed of islands, while the green curve is related to the lower height-level phase which is the uncovered Ge surface. The distance between the centers of two peaks, i.e., the difference in height of the phases, is 1.30 Å, which closely resembles the single atomic step height for Si and Ge (1.36 and 1.40 Å, respectively). At RT the mobility of Si atoms does not seem to be enough to form an ordered structure on top of the Ge substrate, and the Si indiffusion does not occur either. On the other hand, the Ge segregation is limited at RT, as the activation energy for such a process is 1.4 eV [18]. On this basis, we assume that the islands in Fig. 2(b) are formed mostly by Si atoms.

Drastic changes occur after annealing the Si_{1ML}/Ge at 500 °C. First of all, the (2×1) LEED pattern is restored, as clearly seen in Fig. 1(c). As the annealing temperature is far below the temperatures at which Si atoms can desorb from the surface, the recovery of long-range order and initial periodicity on the surface means that either Si atoms substitute the Ge atoms forming the dimers in the topmost layer of substrate or Si atoms diffuse to the bulk. Obviously, in the latter case the Si indiffusion results in the surface becoming terminated by Ge atoms, or in other words, it means Ge segregation, and the top-layer Ge atoms tend to form surface dimers for eliminating the dangling bonds, similar to the dimers on clean Ge(100) surface. Clearly, both mechanisms do not contradict STM results and are able to account for the recovery of the (2×1) structure. Figure 2(d) illustrates an empty-state STM image taken at $V_S = 1.4$ V. At such bias voltage the observed STM features are typical for both Ge(100) and Si(100). The rows of elongated protrusions correspond to the (2×1) structure and those of large protrusions to the local $c(4 \times 2)$ structure with frozen buckled dimers [16,17]. (Note that a local character of the latter structures is the reason why the respective periodicities are not observed in LEED, as already remarked on earlier.) Thus, the annealing at 500 °C enhances the mobility of Si atoms that can incorporate at or below the Ge surface.

Yet, the LEED and STM results in Figs. 1 and 2 cannot answer the question of whether the top-layer dimers of annealed Si_{1ML}/Ge are composed of Si or Ge atoms (or even both, i.e., the dimers could be mixed Si-Ge ones). To gain more information about the atomic structure of annealed Si_{1ML}/Ge, the synchrotron-radiation CL spectroscopy has been utilized in this study. It is well known that even though the CL electrons are highly localized in an atom and cannot take part in bonding directly, their binding energy is sensitive to any changes in surrounding of the atom and associated redistributions of its valence charge [19]. Thus, the aim of this technique is the identification of surface (or interface) related core-level shifts (CLSs), which are caused by rehybridization of surface/interface atoms as compared to the bulk. The CLS measurements can bring the information about the bonding sites and charge states of both Ge and Si atoms at the Si/Ge(100) structures. Moreover, the benefit of synchrotron radiation is that the photon energy can be tuned precisely for the variation of probing depth and optimizing the surface and bulk sensitivity of spectra.

Figure 3 (bottom panel) presents a Ge $3d$ spectrum of the clean Ge(100). The line shape of such spectra is well understood (Ref. [12] and references therein) and can serve a

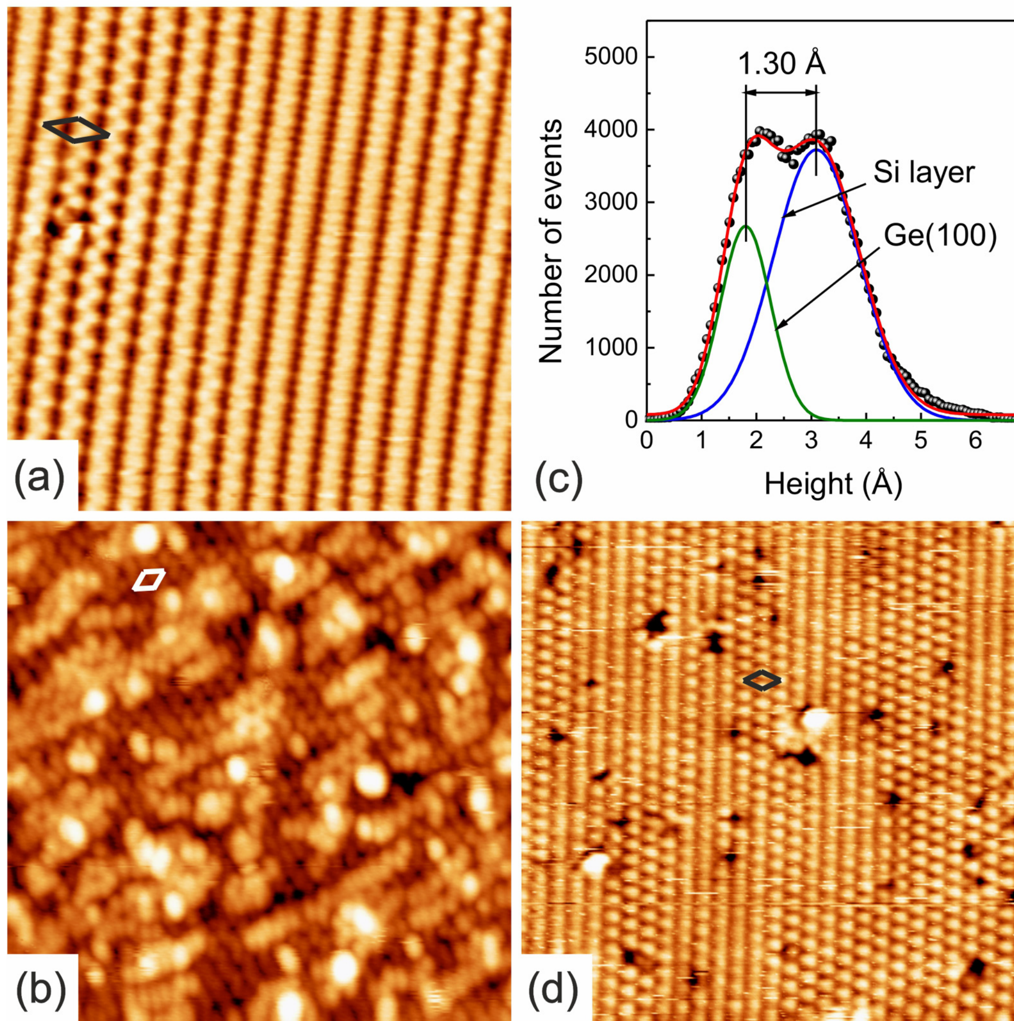

FIG. 2. (a) STM image of the clean Ge(100) surface. The bias voltage (V) is −1.3 V. The tunneling current (I_t) is 0.10 nA. The scanning area is 12.1 × 12.1 nm. (b) STM image of Si_{1ML}/Ge at RT. $V = -1.3$ V and $I_t = 0.10$ nA. The scanning area is 20 × 20 nm. (c) Height distribution plotted for the STM image in (b). Solid curves indicate the fitting results (see the text for details). (d) STM image of Si_{1ML}/Ge after the annealing at 500 °C. $V = 1.4$ V and $I_t = 0.08$ nA. The scanning area is 20.2 × 20.2 nm. The $c(4 \times 2)$ unit cell is outlined in (a), (b), and (d).

reference for the quantitative analysis. The spectrum is taken at $h\nu = 90$ eV (the kinetic energy of photoelectrons around 57 eV) and $\theta_e = 60^\circ$ for the enhancement of surface sensitivity. The raw data (shown by gray symbols) are given after background subtraction by the Shirley method and normalization to the maximum. The spectral analysis is performed by a standard least-squares fitting procedure using a linear combination of spin-orbit Voigt functions. The Lorentzian width (0.150 eV), spin-orbit splitting (0.594 eV), and branching ratio (0.667 ± 10%) were constrained for all components. The variable parameters were CLS, relative intensities, and Gaussian widths (GWs) of components (Table I). The Ge 3*d* line shape of a clean substrate is a convolution of five spin-orbit components shown by filled doublets in Fig. 3. The energy scale on the horizontal axis is aligned to the binding energy of bulk component (labeled *B*) of which the relative binding energy is set to 0 eV. Two surface components shifted by −0.52 eV (Σ_u) and −0.11 eV (Σ_d) relative to *B* have the equal intensities and originate from the top-layer atoms forming buckled dimers, namely the dimer-up and dimer-down atoms, respectively. The third surface component, Σ', which is shifted by −0.20 eV relative to *B*, arises from the second-layer atoms. Finally, a small component L' at 0.51 eV relative to *B* is required to reproduce adequately the higher binding-energy tail of the spectrum. This component is not related to the regular dimer-row reconstruction on the Ge(100) and assumed to originate from surface defects [12]. The total intensity of surface-shifted components (i.e., Σ_u, Σ_d, Σ', and L') is 0.71 and that of *B* is 0.29. The Gaussian width of all components, except for L', is 0.30–0.34 eV. The GW of L' is 0.40 eV, which infers somewhat higher inhomogeneity of Ge sites related to respective defects. The fitting scheme and results described above are fully consistent with earlier studies (Ref. [12] and references therein).

The middle panel of Fig. 3 shows a Ge 3*d* spectrum of Si_{1ML}/Ge at RT. Even though the changes in the Ge 3*d* line shape after the Si deposition are hardly apparent at first glance, this spectrum cannot be decomposed by applying the fitting

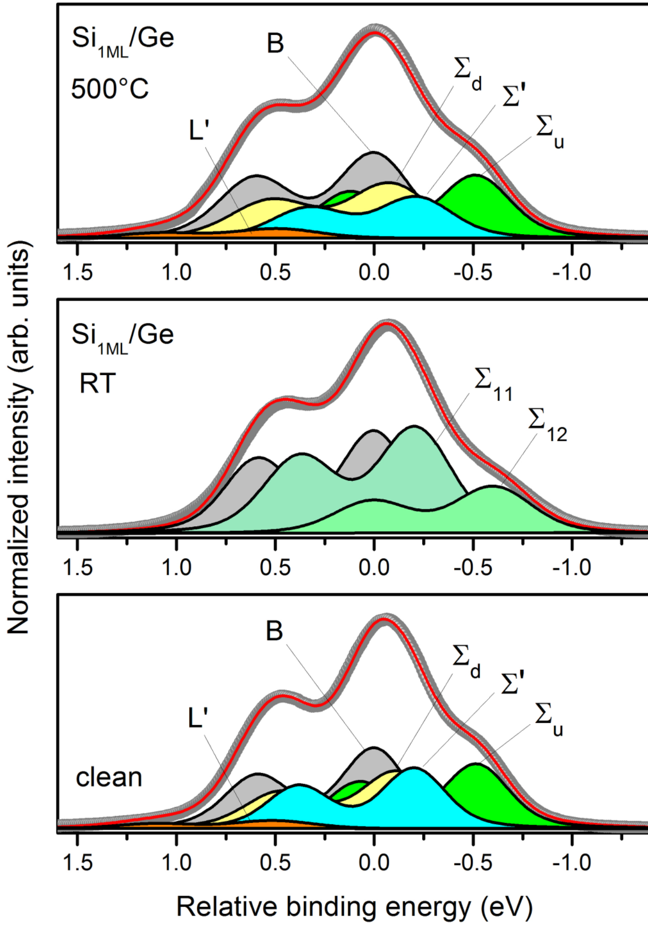

FIG. 3. Ge $3d$ spectra and their deconvolution results for the clean Ge and Si_{1ML}/Ge. The photon energy is 90 eV. The emisson angle is 60 °.

scheme for the clean surface. The curve can be reasonably reproduced with a smaller number of components, namely the bulk and two surface components, Σ_{11} at −0.21 and Σ_{12} at −0.60 eV (Table I). As evidenced from the STM data (Fig. 2), this surface involves two phases, which are the Si islands and uncovered Ge areas. This suggests that the number of bonding sites for Ge atoms is actually more than 2. Hence, we assume that some surface- or/and interface-shifted Ge $3d$ components are hidden because of similarities or proximity of core-level binding energies of Ge atoms at respective sites. Indeed, the GWs of Σ_{11} and Σ_{12} are slightly increased (0.35 and 0.37 eV, respectively) as compared to those of surface components on the clean substrate. This indicates that there might be nonequivalent Ge sites with very similar, albeit not identical, binding energies. Note that the Σ_u and Σ_d components related to the Ge dimers of clean substrate are removed or at least significantly reduced on the Si_{1ML}/Ge at RT. This is in accordance with LEED and STM results in Figs. 1 and 2 showing a gradual disappearing of (2×1) structure. Likewise, the L' is missing, assuming the removal of defect sites characteristic of dimer-row reconstruction on the clean substrate. It is worth noting that due to the difference in electronegativity of Ge (2.0) and Si (1.9), a charge transfer in Ge-Si bonding is expected to occur from Si to Ge. Hence, within the initial-state picture, the CLS of Ge atoms surrounded by Si atom(s) can be expected at a lower binding energy with respect to the CLS of Ge atoms surrounded by Ge atoms. On this basis, one can assume the origins of Σ_{11} and Σ_{12} in Fig. 3. The latter can be interpreted as being due to Ge sites that are efficiently surrounded by Si atoms. Obviously, such sites can be expected for Ge atoms located just below the Si islands. As for the former component, it can be contributed by second-layer Ge atoms and first-layer Ge atoms which are located in between the Si islands.

As seen in Table I, the intensity ratio of Σ_{12} and Σ_{11} is 1:2.1. Neglecting the diffraction effects and taking into account the above considered origins of Σ_{12} and Σ_{11} and the intensities of Σ_u, Σ_d, and Σ' for the clean surface, one can roughly estimate the fraction of Ge surface covered by Si islands. It amounts to ∼0.5–0.6 ML. This is in good agreement with STM results. The total quantity of Ge atoms involved in the reconstructed interface region of the substrate can be estimated from the intensity ratios of surface and bulk components. For the Si_{1ML}/Ge grown at RT, this ratio is 1.63:1 (0.62:0.38). For the clean substrate, this value is 2.45:1 (0.71:0.29). Comparing these ratios, it can be concluded that the quantity of Ge atoms involved in the reconstructed region of Si_{1ML}/Ge is smaller than for the clean substrate. This

TABLE I. Fitting results for Ge $3d$ and Si $2p$ spectra of clean Ge(100) and Si_{1ML}/Ge formed at RT and 500 °C. The spectra are taken at $h\nu = 90$ and 138 eV and $\theta_e = 60^\circ$ and 0 °, respectively. The individual components are shown in parentheses. The CLS are given in eV. The relative intensities of components are presented in brackets. The GWs are between 0.30 and 0.38 eV for most of the components, except for the L', S_{11}, and S_{12} of which GWs are larger than 0.38 eV. See the text for more details.

	Ge(100)	Si_{1ML}/Ge @ RT	Si_{1ML}/Ge @ 500 °C
		Ge $3d$	
(Component)	(B) 0 [0.29]	(B) 0 [0.38]	(B) 0 [0.33]
CLS [intensity]	(Σ_u) −0.52 [0.23]	(Σ_{11}) −0.21 [0.42]	(Σ_u) −0.51 [0.23]
	(Σ') −0.20 [0.21]	(Σ_{12}) −0.60 [0.20]	(Σ') −0.21 [0.16]
	(Σ_d) −0.11 [0.23]		(Σ_d) −0.08 [0.23]
	(L') 0.51 [0.04]		(L') 0.49 [0.04]
		Si $2p$	
(Component)		(S_{11}) 0 [0.80]	(S_{13}) 0.31 [1]
CLS [intensity]		(S_{12}) −0.58 [0.20]	

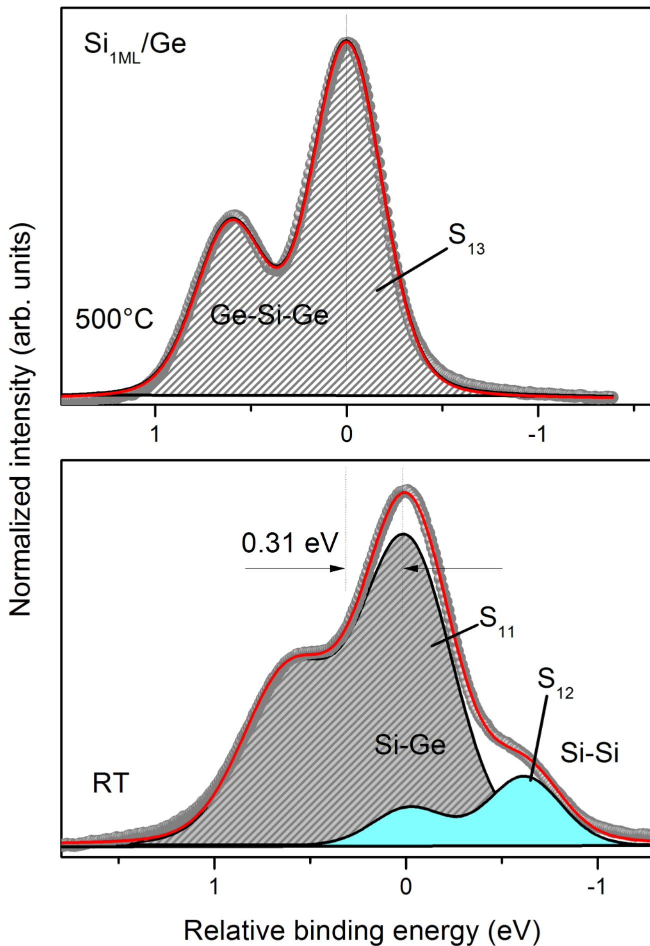

FIG. 4. Si 2p spectra and their deconvolution results for the Si_{1ML}/Ge. The photon energy is 138 eV. The emisson angle is 0 °.

implies that the Ge subsurface layers are practically intact and no Si indiffusion occurs after the Si growth at RT.

The Si structure can be deduced from the analysis of Si 2p spectra. Two spin-orbit components labeled S_{11} and S_{12} are found in the Si 2p spectrum from the Si_{1ML}/Ge at RT, shown at the bottom of Fig. 4. This spectrum is acquired at $h\nu = 138$ eV (the kinetic energy of photoelectrons around 34 eV) and $\theta_e = 0°$. The binding-energy splitting of S_{11} and S_{12} is found to be 0.58 eV. Within the initial-state model, the higher binding-energy component S_{11} (its relative binding energy is set to 0 eV) can be assigned to Si atoms that are more surrounded by Ge atoms and the lower binding-energy component S_{12} to Si atoms that are less surrounded by Ge atoms. In a simplified picture, the former can be assigned to the adsorbed Si atoms that are bonded to the Ge substrate, whereas the latter can stem from the Si atoms that are located on top of Si islands and not bonded to the Ge substrate. As shown in Table I, the intensity ratio of S_{11} and S_{12} is 4:1. Also, it is important that both Si 2p components are broadened as compared to the Ge 3d components. In particular, the GW of S_{11} is 0.52 eV and that of S_{12} is 0.40 eV. Again, this means increased inhomogeneity of the Si layer on this surface, which is fully consistent with the absence of long-range order for Si islands found in the STM image [Fig. 2(b)].

The top panel of Fig. 3 shows a Ge 3d spectrum from the Si_{1ML}/Ge after annealing at 500 °C. Their fitting results are very similar to those of clean substrate (Table I). In particular, the spectrum includes four surface-shifted components, Σ_u, Σ_d, Σ', and L', with their relative intensity ratios similar to those of clean substrate. The recovery of Ge 3d line shape characteristic of the clean Ge clearly indicates that the annealed Si_{1ML}/Ge surface is terminated solely by Ge atoms forming tilting Ge-Ge dimers, while the Si atoms leave the surface and indiffuse beneath, in full agreement with LEED and STM. It is important that the GW of B, Σ_u, Σ_d, Σ', and L' on the Si_{1ML}/Ge is slightly larger (0.33–0.41 eV) than those of clean substrate. Such a broadening is natural in the case of Si indiffusion, leading to additional strain in the Ge lattice and a slightly higher degree of disorder in the segregated topmost Ge layer.

The above conclusions concerning the annealed Si_{1ML}/Ge can be supported also by the analysis of the Si 2p spectrum in Fig. 4 (top panel). It is clearly seen that the Si 2p line shape is very sensitive to the annealing. For the annealed surface, the fitting analysis reveals only a single spin-orbit doublet (labeled S_{13}). It is important that the binding energy of S_{13} is shifted by 0.31 eV toward the higher binding energy relative to the S_{11} component for the unheated Si_{1ML}/Ge at the bottom of Fig. 4. Also, the S_{13} (GW is 0.38 eV) is narrower than both S_{11} and S_{12} in Fig. 4. All this means that after the heating, there is only one type of bonding site for the Si atoms and it is completely different from the Si bonding sites on the unheated surface. Taking into account the above mentioned shift of S_{13} in Fig. 4, one can conclude that the respective Si atoms are more strongly surrounded by Ge ones than the Si atoms which are the origins of S_{11} and S_{12}. Obviously, such a change can be a result of Si indiffusion. Moreover, the fact that all Si sites are equivalent and the narrowing of S_{13} as compared to S_{11} and S_{12} suggest the high homogeneity and good crystallinity of buried Si layer. Most likely, the existence of a well-ordered buried Si layer is the prerequisite for the recovery of (2 × 1) reconstruction on the Ge-segregated Si_{1ML}/Ge(100) surface. Thus, our results show that the annealed Si_{1ML}/Ge(100) represents an example of highly crystalline stack: a well-defined Ge-(2 × 1) /Si_{1ML}/Ge(100) junction with the homogeneous buried Si layer and pure-Ge (2 × 1) reconstruction on top of the sample. Moreover, the crystallinity of the top of this structure, i.e., the well-defined Ge-dimer-row (2 × 1) reconstruction, suggests that the indiffused Si atoms occupy Ge-lattice sites rather than interstitial sites in the Ge host. This infers that the subsurface region is a highly epitaxial $Si_{1-x}Ge_x$ layer with a single Si site.

2. Si_{4ML}/Ge

Figure 5 presents an STM image for the Ge(100) surface after the deposition of 4-ML Si at RT, followed by annealing at 500 °C (Si_{4ML}/Ge hereafter). A LEED pattern from this surface is shown in Fig. 1(d). It reveals the (2 × 1) spots along with the increased intensity of background. As seen in the STM image, the Si_{4ML}/Ge structure appears as a patterned surface with limited dimer rows running along one of two mutually orthogonal directions. Clearly, the difference in morphology of this surface and annealed Si_{1ML}/Ge is related

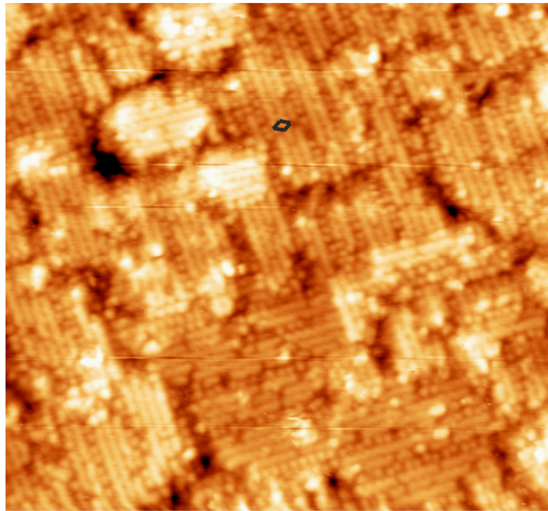

FIG. 5. An STM image of Si_{4ML}/Ge. The bias voltage is −1.4 V. The tunneling current is 0.42 nA. The scanning area is 40.1 × 37.5 nm. The $c(4 \times 2)$ unit cell is outlined.

to different numbers of Si atoms incorporated in the Ge substrate; the increased strain in the Ge lattice is expected in the case of Si_{4ML}/Ge. Thus it is believed that the driving force for the surface patterning is the alloying-induced strain relief. Moreover, it cannot be excluded at this stage that some Si atoms can substitute Ge dimer atoms, leading to the modification of surface structure.

More information about the atomic arrangement of Si_{4ML}/Ge can be gained from CL photoemission. Figure 6 shows Ge 3d and Si 2p spectra from the Si_{4ML}/Ge at two emission angles, $\theta_e = 0^\circ$ and 60°. The fitting results are presented in Table II. The Ge 3d spectrum reveals, in addition to the bulk emission, three interface-related components shifted to the lower binding energy [Σ_{41} (−0.15 eV), Σ_{42} (−0.42 eV), and Σ_{43} (−0.65 eV)] and one component shifted to the higher binding energy [Σ_{44} (0.21 eV)]. In Table II the intensity of such components is provided in brackets for the normal emission angle and braces for the grazing emission angle. It is seen that the Σ_{41} and Σ_{43} are surface sensitive and have equal intensity at both emission angles. Moreover, their binding-energy splitting and CLS relative to B resemble those of Σ_d and Σ_u components originating from the dimer atoms on the clean surface. On this basis, we assign the Σ_{41} and Σ_{43} to dimer-down and dimer-up Ge atoms on the Si_{4ML}/Ge surface. Note that such atoms have slightly larger shifts towards the lower binding energy as compared to the dimer atoms on the clean surface. This can be due to the additional electron charge donated by Si atoms located below the top Ge layer. Also, the energy splitting of Σ_{41} and Σ_{43} is slightly higher (0.50 eV) than that of the clean surface (0.41 eV) (see Table I). Such an increase can indicate a larger charge transfer occurring from the dimer-down to dimer-up atom on the the Si_{4ML}/Ge as compared to the clean surface. Thus, in agreement with STM and LEED, the Si_{4ML}/Ge surface is terminated by Ge-Ge dimers, and the atoms of such dimers have a slightly modified charge state with respect to the dimers on the clean surface.

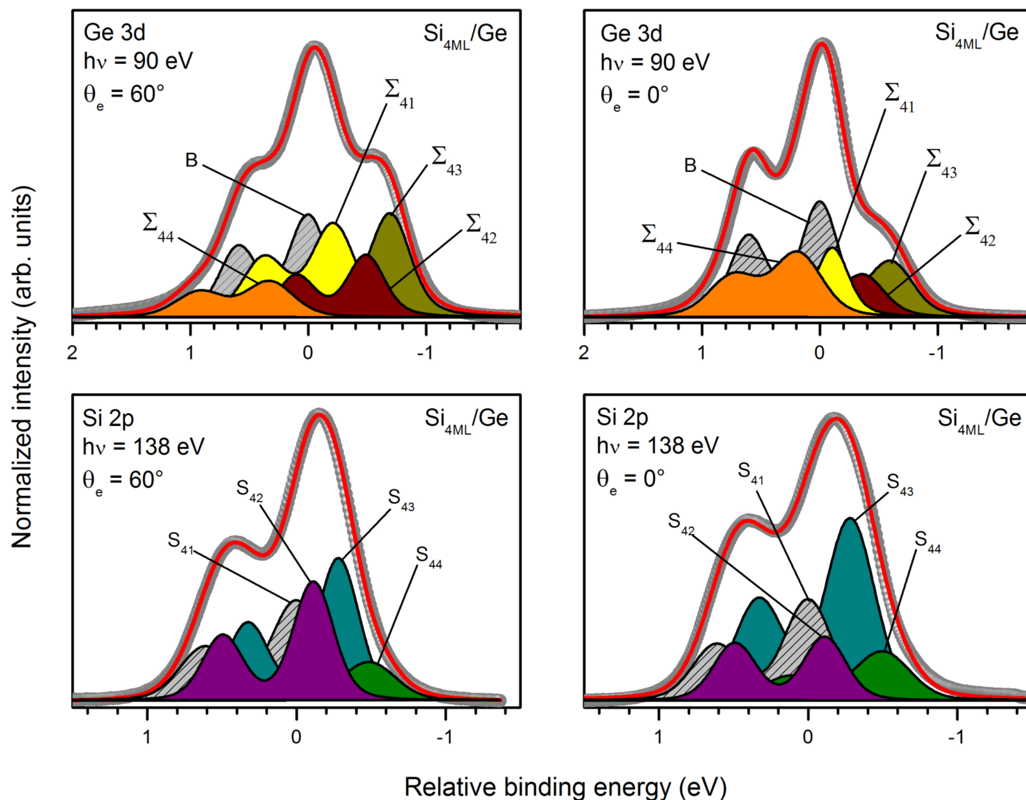

FIG. 6. Ge 3d and Si 2p spectra and their decomposition results for the Si_{4ML}/Ge. The measurements are made at photon energies of 90 and 138 eV, respectively, and two emission angles (0° and 60°).

TABLE II. Fitting results for Ge 3*d* and Si 2*p* spectra of Si_{4ML}/Ge annealed at 500 °C. The spectra are taken at two emission angles (0 ° and 60 °) and photon energy of 90 eV (Ge 3*d*) and 138 eV (Si 2*p*). The individual components are shown in parentheses. The CLS are given in eV. The relative intensities of components are presented in brackets at $\theta_e = 0^\circ$ and braces at $\theta_e = 60^\circ$. The GWs vary between 0.29 and 0.40 eV. See the text for more details.

	Ge 3*d*	Si 2*p*
(Component) CLS	(B) 0 [0.31] {0.23}	(S_{41}) 0 [0.25] {0.28}
[Intensity at $\theta_e = 0^\circ$]	(Σ_{41}) −0.15 [0.17] {0.24}	(S_{42}) −0.11 [0.14] {0.28}
{Intensity at $\theta_e = 60^\circ$}	(Σ_{42}) −0.42 [0.13] {0.16}	(S_{43}) −0.28 [0.47] {0.33}
	(Σ_{43}) −0.65 [0.17] {0.24}	(S_{44}) −0.49 [0.14] {0.11}
	(Σ_{44}) 0.21 [0.22] {0.13}	

Among the other interface-shifted components, the Σ_{42} is essentially less surface sensitive than Σ_{41} and Σ_{43}, and the Σ_{44} has the bulk sensitivity. An appearing of such components is not surprising, since one or more additional Ge sites can be expected as a result of Si indiffusion into the Ge crystal below the top Ge layer and formation of Si-Ge bonds. Thus, the annealed Si_{4ML}/Ge can be considered as the Ge-(2 × 1)/$Si_{1-x}Ge_x$/Ge(100) stack structure where the buried Si-containing layer is an $Si_{1-x}Ge_x$ alloy.

The above conclusion is well supported by the Si 2*p* spectra presented in Fig. 6. They reveal four components, S_{41}, S_{42}, S_{43}, and S_{44}. If the highest binding energy component S_{41} is set to the 0-eV binding energy (the respective Si site is surrounded strongly by Ge atoms), the S_{42}, S_{43}, and S_{44} are shifted towards the lower binding energy side by 0.11, 0.28, and 0.49 eV (Table II). Within the initial-state model, their atomic origins are Si species having fewer Ge neighbors than the Si atoms contributing to the S_{41}. Taking into account the intensities of these components at the two emission angles, the most surface sensitive one is S_{42} and the most bulk sensitive one is S_{43}, while the remaining two are in between. All this infers that the buried $Si_{1-x}Ge_x$ alloy layer includes several Si sites and they are distributed along the ⟨100⟩ direction in a complicated way.

The existence of extra Ge 3*d* components (Σ_{42} and Σ_{44}), in addition to dimer-associated ones (Σ_{41} and Σ_{43}) as well as several Si 2*p* components (S_{41}, S_{42}, S_{43}, and S_{44}) can be also connected with the surface patterning observed in the STM image of Fig. 5. In fact, such patterning is seen to produce a number of grain boundaries between the (2 × 1) patterns, and such boundaries are expected to spread out beneath the surface. A good candidate for the assignment to the grain boundaries is, for example, the Ge 3*d* component Σ_{44}. First of all, it is shifted toward the higher binding energy relative to *B*, similar to the case of the defect-related component L' on the clean surface. Second, the Σ_{44} is bulk sensitive, which is consistent with spreading out the boundaries to the subsurface region. Thus, high-resolution core-level photoemission can allow one to get and resolve a signal from grain boundaries, which is challenging for most techniques without spatial resolution. Moreover, the present study can demonstrate how the existence of grain boundaries is able to broaden the core-level line shape.

Finally, the Si_{1ML}/Ge and Si_{4ML}/Ge structures are similar in that they are both terminated by Ge-Ge dimers but different in that the former includes the homogeneous Si layer with a single bonding site and the latter has the $Si_{1-x}Ge_x$ alloy region with several bonding sites for the Si atoms. The two structures can offer a good platform for a search of templates for enhanced Ge oxidation and improved high-*k*/germanium junctions.

B. Electronic properties

It is known that the *n*-type Ge(100) surface features very strong Fermi level pinning in the band gap at ∼0.08 eV above the VBM [20]. For this reason, it is important to elucidate how the Fermi level position can be influenced by Si/Ge interface structures on top of the *n*-Ge(100). Figure 7 presents VB spectra measured for the clean Ge, Si_{1ML}/Ge, and Si_{4ML}/Ge at $h\nu = 17$ eV. The normal emission angle with the acceptance cone of ±9 ° for the photoelectrons was used, i.e., these spectra bring the information about the electronic structure around the Γ symmetry point of the Brillouin zone. For the clean substrate, at least five features can be identified in the spectrum at 0.44 (S^*), 0.81 (S_1), 1.78 (S_2), 2.87 (S_3), and 3.64 eV (S_4)

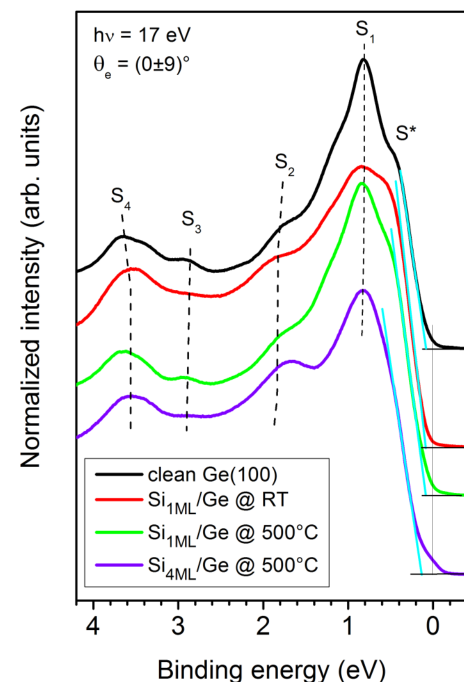

FIG. 7. Valence spectra for the clean Ge, Si_{1ML}/Ge, and Si_{4ML}/Ge. The photon energy is 17 eV. The measurements are made around the Γ symmetry point of the Brillouin zone.

TABLE III. The position of Fermi level above the valence band top (E_F–E_{VBM}) for the *n*-type Ge(100) and Si/Ge structures.

	E_F–E_{VBM} (eV)
Ge(100)	0.08
Si_{1ML}/Ge @ RT	0.08
Si_{1ML}/Ge @ 500 °C	0.08
Si_{4ML}/Ge	0.12

below the Fermi level. This observation is quite consistent with earlier studies [21–24]. The interpretation of these features is not straightforward and is complicated by the fact that they can be contributed by both surface resonances and bulk transitions. Among the above features, the sharp S_1 peak can be ascribed to the dangling-bond band of the down atoms of Ge dimers. Indeed, this peak is prominent for the clean surface as well as Ge-segregated Si_{1ML}/Ge and Si_{4ML}/Ge after the annealing, and depressed for the Si_{1ML}/Ge structure at RT, where the dimer-row reconstruction is significantly removed. The S^* shoulder is prominent for the clean surface and more or less reduced for the Si-deposited surfaces, especially it is almost vanishing for the Si_{4ML}/Ge. Tentatively, this feature can be contributed by surface states related to the Ge backbonds on the clean surface. In contrast, the S_2-S_4 features are practically insensitive to the Si deposition and subsequent annealing. Therefore, they can be strongly contributed by bulk transitions.

The significant influence of bulk on the surface electronic structure of *n*-type Ge(100) is not surprising. It is shown that the state, which is responsible for the strong Fermi level pinning just above the VBM on this surface, has a bulk origin as well [24]. It has been assumed that it is an evanescent state and cannot be removed even by various films grown on Ge [20]. Nevertheless, Fermi level pinning can be completely eliminated by growing epitaxial insulating films on Ge(100), which are matched to the Ge lattice with atomic precision. The position of Fermi level in the band gap can be determined from the VB spectra by extrapolating their linear segments near the VB edge to the zero emission level. The obtained offsets on the binding-energy axis provide the energy difference of Fermi level and VBM. The positions of Fermi level determined from the spectra in Fig. 7 are listed in Table III. It is seen that the formation of Si_{1ML}/Ge structures does not affect Fermi level pinning on the Ge(100) surface. As the dimer-row reconstruction is destroyed in the Si_{1ML}/Ge structure formed at RT, the stability of Fermi level pinning against the Si deposition gives a strong support for the bulk origin of state responsible for this phenomenon.

For the Si_{4ML}/Ge structure, slight alleviation of Fermi level pinning is found. On the other hand, it is worth noting that a band-gap increase can be expected because of the $Si_{1-x}Ge_x$ alloying. It is found at 0.12 eV above the VBM, as shown in Table III. Most likely, the reason for such alleviation is the existence of $Si_{1-x}Ge_x$ interface region on the Si_{4ML}/Ge, which is thicker than that of the Si_{1ML}/Ge. Such a region on the Si_{4ML}/Ge is able to slightly smoothen an abrupt potential step near the Ge interface. While the abrupt potential step on the clean and Si_{1ML}/Ge surfaces is considered to result in states stabilizing the Fermi level on the surface, the smoothening of this step on the Si_{4ML}/Ge is believed to alleviate Fermi level pinning.

C. Interface engineering of advanced Si-Ge structure: Ge-(2 × 1)/$Si_{10\times 1ML}$/Ge(100)

The preceding results (Sec. III A) demonstrate the potential of Si-Ge interface structures for the fabrication of high-*k*/Ge junctions with improved properties. First of all, the incorporation of the Si layer into the Ge substrate allows one to control Ge oxidation [8,9]. Moreover, the amount of deposited Si can affect Fermi level pinning, leading to the junctions with tailored electronic properties. However, the increase in the number of bonding sites for Si and Ge atoms (including defect sites) in the $Si_{1-x}Ge_x$ alloy interfaces with the deposited Si amount can apply a limit for using such systems as templates for high-*k*/Ge junctions. In fact, the increased number of structural defects is usually associated with the additional electronic states in the band gap (i.e., defect-type gap states), which hinders the device performance. In this context, the Ge/Si_{1ML}/Ge(100) appears to be an ideal model template, because such interface possesses a high degree of abruptness, crystallinity, and homogeneous Si sites. On the other hand, the Si amount at this interface might not be enough for efficient Ge passivation by capping oxide layer. Hence, the increase of Si amount without breaking the useful properties of Ge/Si_{1ML}/Ge(100) is required for the synthesis of improved template.

In this study, we propose an interface-engineering method for the synthesis of an improved Si-Ge template. Based on the results in Sec. III A, one can construct an advanced Ge/ $Si_{1-x}Ge_x$/Ge(100) structure which has a high degree of crystallinity and large Si quantity simultaneously. Since the indiffusion of Si monolayer, deposited on the Ge(100)(2 × 1) at RT annealed afterwards, leads to a homogeneous Si layer beneath and segregated Ge-dimer (2 × 1) top layer, a key idea of this method is the Si deposition by limited portions (one dose is 1 ML) at RT, which are followed by annealing. Here we demonstrate a significant improvement in smoothness, homogeneity, and crystallinity of Si/Ge interface structure, when it is produced by series of 1-ML Si depositions with subsequent anneals as compared to the Si/Ge structure where the whole amount of Si is directly deposited at once, followed by the heating. In other words, we have compared two cases: (i) 10 MLs of Si atoms are directly deposited on the clean Ge(100) and the sample is annealed at 600 °C afterwards, and (ii) the same amount of Si atoms is deposited by several portions (1 ML each, ten portions total), with the annealing at 600 °C being performed after depositing each portion.

Figure 8(a) shows an STM image of Si/Ge structure after the deposition of 10 MLs of Si atoms on the Si(100) and subsequent annealing at 600 °C. It is seen that the surface is rough and includes random clusters of arbitrary shape and size. No diffraction spots are found for this surface in LEED. The surface morphology can be characterized by height distribution illustrated in Fig. 8(b). The roughness curve has an asymmetric line shape and can be fitted by two Gaussian peaks with GWs of 2.67 and 5.60 nm. This implies that the surface is comprised of two phases,

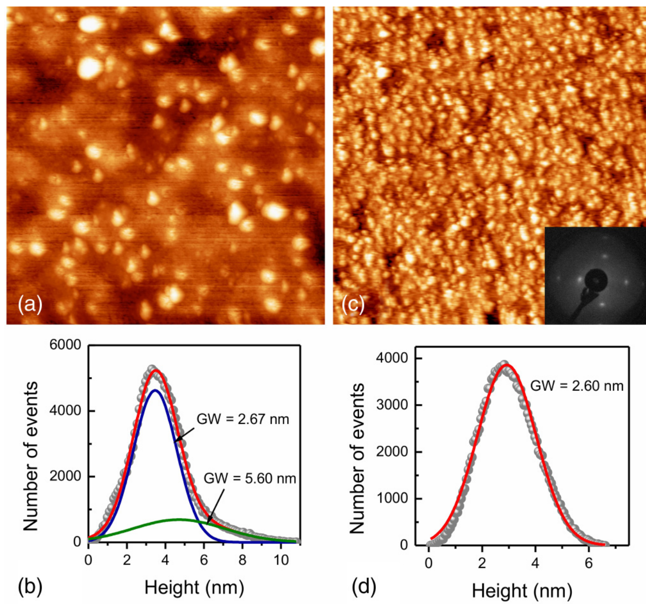

FIG. 8. (a) An STM image of Si/Ge structure formed by deposition of 10-ML Si at RT and subsequent annealing at 600 °C. The bias voltage is 2.0 V. The tunneling current is 0.5 nA. The scanning area is 400 × 400 nm. (b) Height distribution plotted for the image in (a). The fitting results are shown by solid curves. (c) An STM image of Si/Ge structure formed by Si deposition by portions of 1 ML each at RT and annealings at 600 °C after each deposition. The bias voltage and tunneling current are the same as for the image in (a). The scanning area is 300 × 300 nm. (d) Height distribution for the image in (c). The fitting results are presented by solid curve.

one of which is assumed to be an $Si_{1-x}Ge_x$ alloy with a lower roughness and the other pure Si islands with a higher roughness.

Figure 8(c) presents an STM image for the Ge surface at which the equivalent Si amount is incorporated by the above method. Namely, ten portions of Si atoms (1 ML each) are deposited with anneals at 600 °C after each deposition. Figure 9 shows test XPS spectra taken after the sixth and tenth cycles of growth. Comparing the two spectra, it is seen that the Si 2*p* peak increases by 62% and the Ge 3*d* peak decreases by 17%. As seen from the STM image of Fig. 8(c), the top of the structure prepared by series of Si depositions is much more uniform and smooth. The roughness analysis [Fig. 8(d)] shows that the height distribution of this surface can be reasonably fitted with a single Gaussian peak. Its width is 2.60 nm, which is close to the height distribution width for the surface Si-Ge alloy phase in Fig. 8(a) (2.67 nm). The phase interpreted as originating from the Si clusters is absent in Fig. 8(c). Therefore, the method allows us to incorporate the whole Si amount (10 MLs) into the Ge interface more efficiently. Moreover, the LEED demonstrates the (2 × 1) pattern for this surface. Thus, utilizing the interface-engineering method, we are able to produce a crystalline Si-Ge interface with tailored properties (with the increased Si amount and lowered density of defects). Such an interface is a promising candidate for a template for growing advanced high-*k*/Ge systems. In the near future, systems with such a template will be tested.

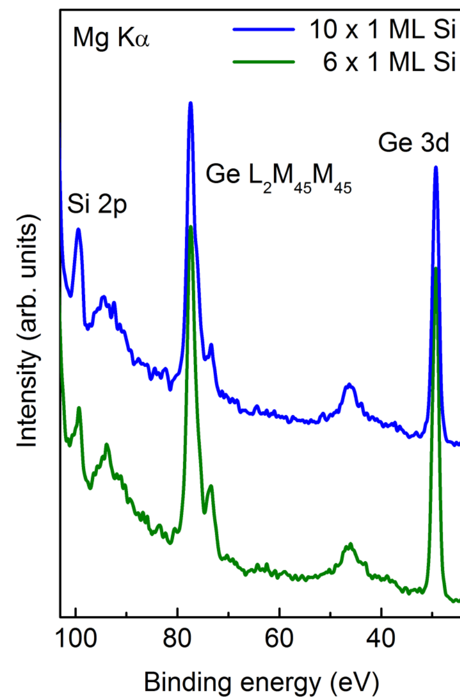

FIG. 9. XPS spectra for $Ge/Si_{6\times 1ML}/Ge$ and $Ge/Si_{10\times 1ML}/Ge$ structures.

IV. CONCLUSIONS

Using LEED, STM, XPS, and photoelectron spectroscopy using synchrotron radiation, the initial stages of formation and structural and electronic properties of Si/Ge interfaces produced at amounts of deposited Si atoms and different substrate temperatures have been studied. At RT, the Si in-diffusion below the top Ge layer does not occur, and the Ge surface is covered by structureless Si islands breaking the native (2 × 1) dimer-row reconstruction. Such an interface is metastable, and upon annealing at 500 °C, thermally induced transformation of Si/Ge is found. In particular, the Si atoms diffuse below the top layer, while Ge atoms segregate on the surface and restore the (2 × 1) dimer-row structure. After such intermixing, the structure of buried Si-containing layer and number of Si sites are dependent on the amount of deposited Si atoms. For the 1-ML coverage, the Si atoms form the homogeneous layer with equivalent bonding sites, resulting in the highly crystalline Ge-(2 × 1)/$Si_{1-x}Ge_x$/Ge(100) stack. For the 4-ML coverage, the top of interface is still covered with Ge-Ge dimers, while the number of bonding sites for the indiffused Si atoms drastically increases, and the $Si_{1-x}Ge_x$ alloy is found below the top Ge layer. It is found that on such a surface, the Ge-Ge dimers are buckled, but the charge state of dimer atoms and the electron charge transfer between them are slightly different from those of the clean Ge surface, which is explained by the donation of electron charge from the neighboring indiffused Si atoms. The electronic structure of these interfaces has to a large extent remained intact, since it is strongly contributed by the Ge bulk. In particular, Fermi level pinning is not affected by the deposition of 1-ML Si at all, and only weak alleviation of this phenomenon occurs in the case of 4-ML Si.

Finally, on the basis of knowledge about the structural and electronic properties and initial stages of formation of Si/Ge structures, a method is proposed for the atomic-level engineering of advanced Si/Ge interfaces with a high degree of crystallinity and a relatively large amount of incorporated Si atoms, which can be a promising candidate as templates for growing improved high-k/Ge junctions. The Ge-$(2 \times 1)/\mathrm{Si}_{10\times 1\mathrm{ML}}$/Ge(100), a stack prepared by using this method, is compared with the standard Si/Ge structure which is formed by the deposition of 10 MLs on Ge(100), followed by the annealing. It is found that the former stack, in contrast to the latter one, exhibits the long-range order and more homogeneous and smooth surface morphology.

ACKNOWLEDGMENT

We thank the MAX-lab staff for their assistance.

[1] Y. M. Haddara, P. Ashburn, and D. M. Bagnall, Silicon-Germanium: Properties, growth and applications, in *Springer Handbook of Electronic and Photonic Materials*, edited by S. Kasap and P. Capper (Springer, Cham, 2017), Chap. 22, p. 523.

[2] D.-S. Lin, T. Miller, and T.-C. Chiang, Phys. Rev. B **45**, 11415 (1992).

[3] A. A. Stekolnikov, J. Furthmüller, and F. Bechstedt, Phys. Rev. B **65**, 115318 (2002).

[4] S. J. Jenkins and G. P. Srivastava, Phys. Rev. B **57**, 8794 (1998).

[5] W.-H. Tu, C.-H. Lee, H. T. Chang, B.-H. Lin, C.-H. Hsu, S. W. Lee, and C. W. Liu, J. Appl. Phys. **112**, 126101 (2012).

[6] F. E. Leys, R. Bonzom, B. Kaczer, T. Janssens, W. Vandervorst, B. De Jaeger, J. Van Steenbergen, K. Martens, D. Hellin, J. Rip, G. Dilliway, A. Delabie, P. Zimmerman, M. Houssa, A. Theuwis, R. Loo, M. Meuris, M. Caymax, and M. M. Heyns, Mater. Sci. Semicond. Process. **9**, 679 (2006).

[7] A. Dimoulas, P. Tsipas, A. Sotiropoulos, and E. K. Evangelou, Appl. Phys. Lett. **89**, 252110 (2006).

[8] Y. Kamata, Mater. Today **11**, 30 (2008).

[9] R. M. Wallace, P. C. McIntyre, J. Kim, and Y. Nishi, MRS Bull. **34**, 493 (2009).

[10] N. W. Hendrickx, I. L. W. Lawrie, M. Russ, F. van Riggelen, S. L. de Snoo, R. N. Schouten, A. Sammak, G. Scappucci, and M. Veldhorst, Nature (London) **591**, 580 (2021).

[11] I. Horcas, R. Fernández, J. M. Gómez-Rodríguez, J. Colchero, J. Gómez-Herrero, and A. M. Baro, Rev. Sci. Instrum. **78**, 013705 (2007).

[12] M. Kuzmin, M. P. J. Punkkinen, P. Laukkanen, R. E. Perälä, J. J. K. Lång, J. Dahl, J. Adell, and K. Kokko, Surf. Sci. **615**, 88 (2013).

[13] D. J. Chadi, Phys. Rev. Lett. **43**, 43 (1979); J. Ihm, M. L. Cohen, and D. J. Chadi, Phys. Rev. B **21**, 4592 (1980).

[14] J. Pollmann, P. Kruger, and A. Mazur, J. Vac. Sci. Technol. B **5**, 945 (1987).

[15] A. van Houselt, R. van Gastel, B. Poelsema, and H. J. W. Zandvliet, Phys. Rev. Lett. **97**, 266104 (2006).

[16] Y. Takagi, K. Nakatsuji, Y. Yoshimoto, and F. Komori, Phys. Rev. B **75**, 115304 (2007).

[17] Y. Takagi, Y. Yoshimoto, K. Nakatsuji, and F. Komori, Surf. Sci. **559**, 1 (2004); **593**, 133 (2005).

[18] D. J. Godbey and M. G. Ancona, Surf. Sci. **395**, 60 (1998).

[19] E. Pehlke and M. Scheffler, Phys. Rev. Lett. **71**, 2338 (1993).

[20] M. Kuzmin, P. Laukkanen, J. Mäkelä, M. Tuominen, M. Yasir, J. Dahl, M. P. J. Punkkinen, and K. Kokko, Phys. Rev. B **94**, 035421 (2016).

[21] E. Landemark and R. I. G. Uhrberg, Surf. Sci. Lett. **236**, L359 (1990).

[22] E. Landernark, C. J. Karlsson, L. S. O. Johansson, and R. I. G. Uhrberg, Phys. Rev. B **49**, 16523 (1994).

[23] A. Santoni and V. R. Dhanak, Surf. Sci. **537**, L423 (2003).

[24] H. Seo, R. C. Hatch, P. Ponath, M. Choi, A. B. Posadas, and A. A. Demkov, Phys. Rev. B **89**, 115318 (2014).